Dynamics of the Forced Josephson Junction Circuit: The Regions of Chaos

FATHI M. A. SALAM AND S. SHANKAR SASTRY

Abstract—**We study the dynamics of the Josephson junction circuit with both dc and ac current forcing, with emphasis on the ac case. Specifically, we derive analytically the bifurcation diagram of the small amplitude ac forced Josephson junction. We thus place on analytic grounds the qualitative, experimental, and simulation work of Belykh, Pedersen, and Soerensen; specially that which pertains to the regions of chaos. Combining previous results from the literature with our new results, we provide an enhanced picture of the dynamics of the ac forced case, as well as insightful explanation of the associated $I-V$ characteristics. Explicit asymptotic formulae for the curves that separate the different regions in the bifurcation diagram are also given.**

I. Introduction

THE dynamics of the Josephson junction circuit is studied with both dc and ac forcing, with emphasis on the ac case [19], [20]. Specifically, *we derive analytically the bifurcation diagram of the ac forced Josephson junction* with small forcing, as well as the associated $I-V$ characteristics. We place on firm analytic ground the qualitative, experimental, and simulation work of Belykh, Pedersen, and Soerensen [7], specially that which pertains to regions of chaos. Abidi and Chua [3] and Odyniec and Chua [13], [14] have supplied analytic treatment in the case when the Josephson junction possesses periodic (rotational) orbits. We utilize their results, as well as ours, to provide a comprehensive picture of the total dynamics of the small amplitude ac forced case and its implications for the associated $I-V$ characteristics.

The key to realizing the afore mentioned program of obtaining the ac bifurcation diagram is to prove analytically the existence of chaos for certain parameter values, in the dynamics of the ac forced junction.[1] Chaos, i.e., complex orbital behavior, occurs in many systems of practical interest. In addition to a huge volume of simulation evidence, chaos has been analytically shown to exist, for instance, in the Duffing equation (Greenspan and Holmes [8]), the swing equations of a power system (Kopell and Washburn [12], Salam, Marsden, and Varaiya [2]). It would appear superficially that the results presented in [2] (evidence of the Arnold diffusion variety of chaos) which are valid for system equations associated with the dynamics of forced pendula, can readily be transcribed to the present case. Certainly the dynamics of the forced junction are those of a forced pendulum. The difference, however, lies in the fact that the damping associated with these dynamics (their departure from being Hamiltonian) is not necessarily small—this necessitates several non-trivial modifications in the theory presented in [10], [9], [1], [2]. We prove the existence of "Smale–Birkhoff horseshoe" chaos in the dynamics of the Josephson junction using the method of Melnikov thereby supporting the experimental and simulation results of [6], [7], [11] in the 10–300-GHZ range.

We point out that other mechanisms, such as period doubling, overlapping of resonances, etc., may generate chaos for the same or different parameter ranges from the ones obtained here. This is to say, we are only considering one route to chaos, namely the (transversal) homoclinic route.

The outline of our paper and our contributions are as follows: In Section II we review the model of the Josephson junction dynamics. We briefly review the bifurcation diagram of the dc forced junction derived in [17] (and described in [3], [7], [13]) as well as the $I-V$ characteristics of the dc forced junction. We then explain the ac bifurcation diagram of [7] obtained by simulation, experiment and qualitative arguments. We describe the region of the ac dynamics which has been studied by Odyniec and Chua in [13], [14]—they explain essentially the piecewise-constant portion of the $I-V$ characteristic in the ac forced junction.

We point out in Section II, the need for analytic proofs for the existence of chaos in certain parameter ranges to analytically confirm the conjecture of [7]. To this end, we begin with a brief discussion of chaos and the Melnikov technique for establishing the presence of a Smale–Birkhoff horseshoe in the dynamics of a periodically forced nonlinear system. We do not review the results on the specifics of the chaos associated with the horseshoe here—the reader is referred to the papers of Kopell and Washburn [12], Salam, Marsen, and Varaiya [1], Greenspan and Holmes [8], Holmes [10], and the new book of Guckenheimer and Holmes [9] for this. In Sections IV and V we apply these techniques to establish the existence of "horseshoe" chaos

Manuscript received October 4, 1983; revised June 4, 1984; and December 3, 1984. F. M. A. Salam was supported by a Drexel University Grant of June–July 1983, and by the National Science Foundation under Grant ECS-8404723. S. S. Sastry was supported by a Regents Junior Faculty Fellowship of June–July 1983.

F. M. A. Salam is with the Department of Mechanical Engineering and Mechanics, Systems Group, Drexel University, Philadelphia, PA 19104.

S. S. Sastry is with the Department of Electrical Engineering and Computer Sciences, University of California, Berkeley, CA 94720.

[1]Specifically we prove the existence of transversal homoclinic points, which in turn imply the existence of Birkhoff–Smale horseshoes.

0098-4094/85/0800-0784$01.00 ©1985 IEEE

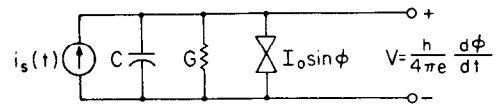

Fig. 1. Josephson junction circuit model.

in the junction for different sets of parameter ranges—Section IV deals with junctions with low conductance and dc current values; whereas Section V has no such restriction. In Section IV the junction's model becomes near-Hamiltonian[2] and this facilitates the derivation of explicit asymptotic formulas that approximate the boundaries of the chaotic regions in the space of parameters.

We point out that the treatment of chaos, using the Melnikov technique, generally involves certain technicalities. Specifically, one must show the following: (1) the derived improper (Melnikov) integrals exist and are finite, and as in the Josephson-junction case, (2) these integrals do not equal zero simultaneously, in order to conclude the existence of "horseshoe" chaos. These technical questions, directly or indirectly, must be verified as will be shown in the context of Sections IV and V.

In Section VI, we collect all the results to analytically derive the complete ac bifurcation diagram of the junction and the relation between the ac and dc bifurcation diagram. We close the section with a discussion of the effect on our analysis of increasing the amplitude of the ac forcing of the junction beyond its "very small" value.

For a good description of recent advances in superconducting devices and circuits see Van Duzer and Turner [16]. Further, the presence of chaos in the junction dynamics is believed to result in increased noise observed at the junction as discussed in [6], [7], [11]. This is particularly of consequence when the junction is used in mixer applications.

II. Dynamics of the Josephson Junction

2.1. The Model

The dynamics of a Josephson junction driven by a current source, as shown in Fig. 1 (see, e.g., [3], [6], [7], [11], [13], [16]), satisfies the following differential equation:

$$\frac{hC}{4\pi e}\frac{d^2\phi}{dt^2}+\frac{hG}{4\pi e}\frac{d\phi}{dt}+I_0\sin\phi=i_s(t). \tag{2.1}$$

Here h is Planck's constant, e the electronic charge, I_0 a threshold current associated with the tunnelling current, C the junction capacitance, G the junction conductance, and ϕ the difference in phase of the order parameters across the junction. The junction voltage v is given by

$$v=\frac{h}{4\pi e}\frac{d\phi}{dt}. \tag{2.2}$$

[2]After our report [19] was prepared, we learned of the work by Genchev *et al.* [21] where the Melnikov technique was applied to the model of Section IV here. Still there are differences: in [21] the application was to the upper heteroclinic curve only. Although we have used the Melnikov technique in Section IV to establish horseshoe chaos, our primary interest is in deriving the asymptotic bifurcation formulas that identify the regions of chaos in the parameter space.

Equation (2.1) may be rescaled so as to make it dimensionless as follows: set

$$\tau=\frac{4\pi eI_0}{hG}t, \qquad \beta=\frac{4\pi eI_0}{h}\frac{C}{G^2}$$

and

$$\bar{i}_s(\tau)=\frac{1}{I_0}i_s\left(\frac{hG}{4\pi eI_0}\tau\right).$$

Then (2.1) reads as

$$\beta\ddot{\phi}+\dot{\phi}+\sin\phi=\bar{i}_s(\tau) \tag{2.3}$$

with $\dot{\phi}=d\phi/d\tau$, $\ddot{\phi}=d^2\phi/d\tau^2$. The form of the scaling (2.3) is not standard (it is degenerate when $G=0$). Sometimes an alternate scaling of (2.1) is useful. Define

$$t'=\left(\frac{4\pi eI_0}{hC}\right)^{1/2}t; \qquad d=\left(\frac{h}{4\pi eI_0C}\right)^{1/2}G;$$

and

$$i_s'(t')=\frac{1}{I_0}i_s\left(\left(\frac{hC}{4\pi eI_0}\right)^{1/2}t'\right)$$

to obtain

$$\ddot{\phi}+d\dot{\phi}+\sin\phi=i_s'(t') \tag{2.4}$$

(this scaling is degenerate when $C=0$). The form (2.4) is useful in some contexts since d has the physical interpretation of damping. Note that β of (2.3) is equal to $1/d^2$. Note further that when $i_s(t)=I_{dc}+\epsilon I_{ac}'\sin\omega t$, we have

$$\bar{i}_s(\tau)=\frac{1}{I_0}\left[I_{dc}+\epsilon I_{ac}'\sin\omega\left(\frac{hG}{4\pi eI_0}\right)\tau\right]$$
$$:=\rho+\epsilon A'\sin\bar{\omega}\tau$$
$$i_s'(t')=\frac{1}{I_0}\left[I_{dc}+\epsilon I_{ac}'\sin\omega\left(\frac{hC}{4\pi eI_0}\right)^{1/2}t'\right]$$
$$:=\rho+\epsilon A'\sin\omega' t'$$

where $\omega'=\bar{\omega}/d$ and $0<\epsilon\ll 1$ (set $I_{ac}:=\epsilon I_{ac}'$, $A:=\epsilon A'$ where I_{ac} and $A'>0$). Here we will use both models (2.3) and (2.4) as convenient.

2.2. Constant Forcing (DC Analysis)

Equation (2.3) has been studied extensively in the instance that $i_s(\tau)=\rho$, (equivalently, $i_s(t)=I_{dc}$), as the equation by Andronov, Khaiken, and Vitt [4], Levi, Hoppensteadt, and Miranker [17], Belykh, Pedersen, and Soerensen [7], Abidi and Chua [3], Odyniec and Chua [13] and in the context of the swing equation of a power system by Arapostathis, Sastry, and Varaiya [5]. We review the results briefly: rewriting (2.3) with $\dot{\phi}=y$ and $\bar{i}_s(\tau)=\rho$ as first-order system we have

$$\dot{\phi}=y, \qquad \dot{y}=\frac{-y-\sin\phi+\rho}{\beta}. \tag{2.5}$$

Equation (2.5) is periodic in ϕ. Consequently, the state (ϕ, y) can be viewed either as an element of $R\times R$ or $S^1\times R$ where $S^1=[0,2\pi]$ with 0, 2π identified. The state space $S^1\times R$ is more natural, but we use both $R\times R$ and $S^1\times R$ as per convenience.

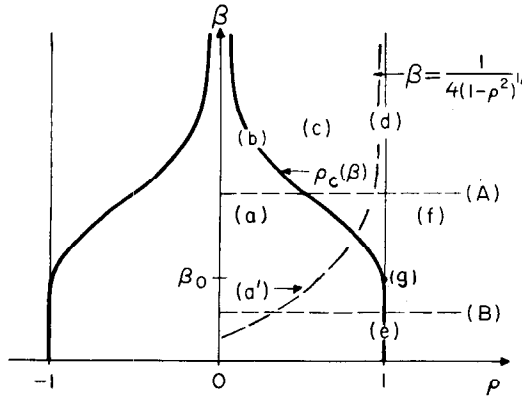

Fig. 2. Bifurcation diagram for (2.5).

2.2.1. Bifurcation Diagram for the DC Excited Junction: The bifurcation diagram of (2.5) with ρ, β as parameters is shown in Fig. 2 (for $\beta > 0$). The diagram is symmetric about the β-axis so that we will discuss it only for positive values of ρ. In the region (a), (2.5) has two equilibrium points in $S^1 \times R$; the one a node and the other a saddle. All trajectories converge to one or the other equilibrium point as shown in Fig. 3(a). We have also drawn the phase portrait Fig. 3(a') for the region (a') when

$$\beta \leqslant \frac{1}{4(1-\rho^2)^{1/2}}. \tag{2.6}$$

The curve (2.6) is shown dotted in Fig. 2. The phase portrait of Fig. 3(a') is homeomorphic to Fig. 3(a)—the only difference between the two being that the stable equilibria of Fig. 3(a') are sinks (real eigenvalues of linearization) rather than foci (complex eigenvalues of linearization) as in Fig. 3(a). In the region (c), (2.5) has two equilibrium points and a stable periodic orbit on $S^1 \times R$. As shown in Fig. 3(c), the stable periodic orbit on $S^1 \times R$ corresponds to an unbounded trajectory on $R \times R$—such a periodic orbit is known as a *rotation*. A trajectory that forms a periodic orbit both on $S^1 \times R$ and on $R \times R$ is referred to simply as an *oscillation* to distinguish it from a rotation. In the region (f) (2.5) has only a stable periodic orbit—a rotation, see Fig. 3(f). The curves separating regions (a), (c) and (f) are the bifurcation curves—(b) := $\{(\rho, \beta)$: $\rho = \rho_c(\beta)$, $\beta > \beta_0\}$, (d) := $\{(\rho, \beta)$: $\rho = 1$, $\beta > \beta_0\}$, and (e) := $\{(\rho, \beta)$: $\rho = 1$, $\beta < \beta_0\}$; these curves are (smoothly) connected by the point (g) := $\{\rho = 1, \beta = \beta_0\}$. On (b), the phase portrait of (2.5) includes two equilibrium points and a *saddle connection* as shown in Fig. 3(b). On (d), the phase portrait includes a single equilibrium point obtained by the fusion of the saddle and the node (a *saddle-node* bifurcation) and a rotation as shown in Fig. 3(d). At the point (g), the saddle node and saddle connection occur simultaneously.

In the region (e) below (g) on the line $\rho = 1$, we have a trajectory joining fused saddle-nodes as shown in Fig. 3(e). The phase portrait arises from the coalescence of the equilibria of Fig. 3(a') into a saddle sink connection.[3]

[3] One of the reviewers suggested that the analyses used in [22] may be useful in the study of this part of the parameter space.

The sequence of bifurcations obtained when ρ is increased for a fixed value of β is illustrated by the two horizontal lines (A) and (B) in Fig. 2. Line (B) corresponds to a small value of β (consequently, large damping (d)) and line (A) to an intermediate value of β. Traversing line (A) in the direction of increasing ρ starting from $\rho = 0$, one successively obtains the phase portraits shown in Fig. 3(a)–(d), and (f). Traversing line (B) in the direction of increasing ρ, one obtains the phase portraits of Fig. 3(a), (a'), (e), and (f).

2.2.2. I–V Characteristics of the DC-Excited Junction: While the bifurcation diagram of Fig. 2 gives the complete portrait of the dynamics, one is often interested for applications in an I–V characteristic, i.e., a plot of I_{dc} (proportional to ρ, specifically $I_{dc} = I_0\rho$) versus V_{av} (proportional to the time averaged value of $y = d\phi/d\tau$, specifically $h/2\pi e\langle d\phi/d\tau\rangle$). Consider first a junction which has an intermediate value of β, say, β at line (A) in the bifurcation diagram of Fig. 2. We study the V_{av} versus I_{dc} curve as I_{dc} (or equivalently ρ) is gradually (quasi-statically) increased from zero, i.e., we traverse the line (A) in the bifurcation diagram. Initially, we are in region (a); all trajectories converge to one of the two equilibrium points on $S^1 \times R^1$. Since, $y = 0$ at each of these points (of course, it is extremely unlikely that the trajectory will converge to the saddle equilibrium point); the steady state value of the voltage V or $V_{av} = 0$. When ρ increases above the value $\rho_c(\beta)$, we are in region (c), where there is both a rotation and two equilibrium points on $S^1 \times R^1$. However, in the experiment that is being performed (increasing I_{dc} gradually), the initial conditions for the system (2.5) will be in the domain of attraction of the stable equilibrium point and consequently the trajectory will converge to the steady state value of zero. Finally, when ρ exceeds 1; the equilibria annihilate each other in a saddle-node leaving only the stable rotation. All trajectories then converge to the rotation (in region (f)) where the average value of y, i.e. V_{av}, $\neq 0$. This explains the jump in the characteristic of Fig. 4(a). In this figure, we show the jump occurring at $I_{dc} = I_0$ (i.e., $\rho = 1$), though, in an actual experiment, the jump may occur slightly before I_0.

We now explain the hysteresis in the characteristic of Fig. 4(a), corresponding to gradually reducing ρ (and I_{dc}) from values of $\rho > 1$ (region (f)) along the horizontal line (A) in Fig. 2. As ρ is reduced below 1, the two equilibria reappear; but initial conditions are such as to cause the trajectory to converge to the rotation, now in region (c). At $\rho = \rho_c(\beta)$, the rotation is destroyed in a saddle-connection leaving only the equilibria and consequent convergence of all trajectories to points where the average value of $y = 0$. This explains the hysteretic jump in the characteristic at $I_{dc} = I_{dc}(\beta)$ (i.e., $\rho = \rho_c(\beta)$). In [15] it has been shown that $\langle y\rangle$ is a monotone function of $\rho > \rho_c(\beta)$.

The diagram of Fig. 4(b) corresponds to a junction with a fixed low value of $\beta < \beta_0$. Consider again the experiment of gradually increasing ρ (along line (B) in Fig. 2. For $\rho < 1$, we are in region (a) and $V_{av} = 0$. For $\rho > 1$, we are in region (f) and V_{av} is nonzero. For decreasing ρ; exactly the opposite takes place and there is no hysteresis.

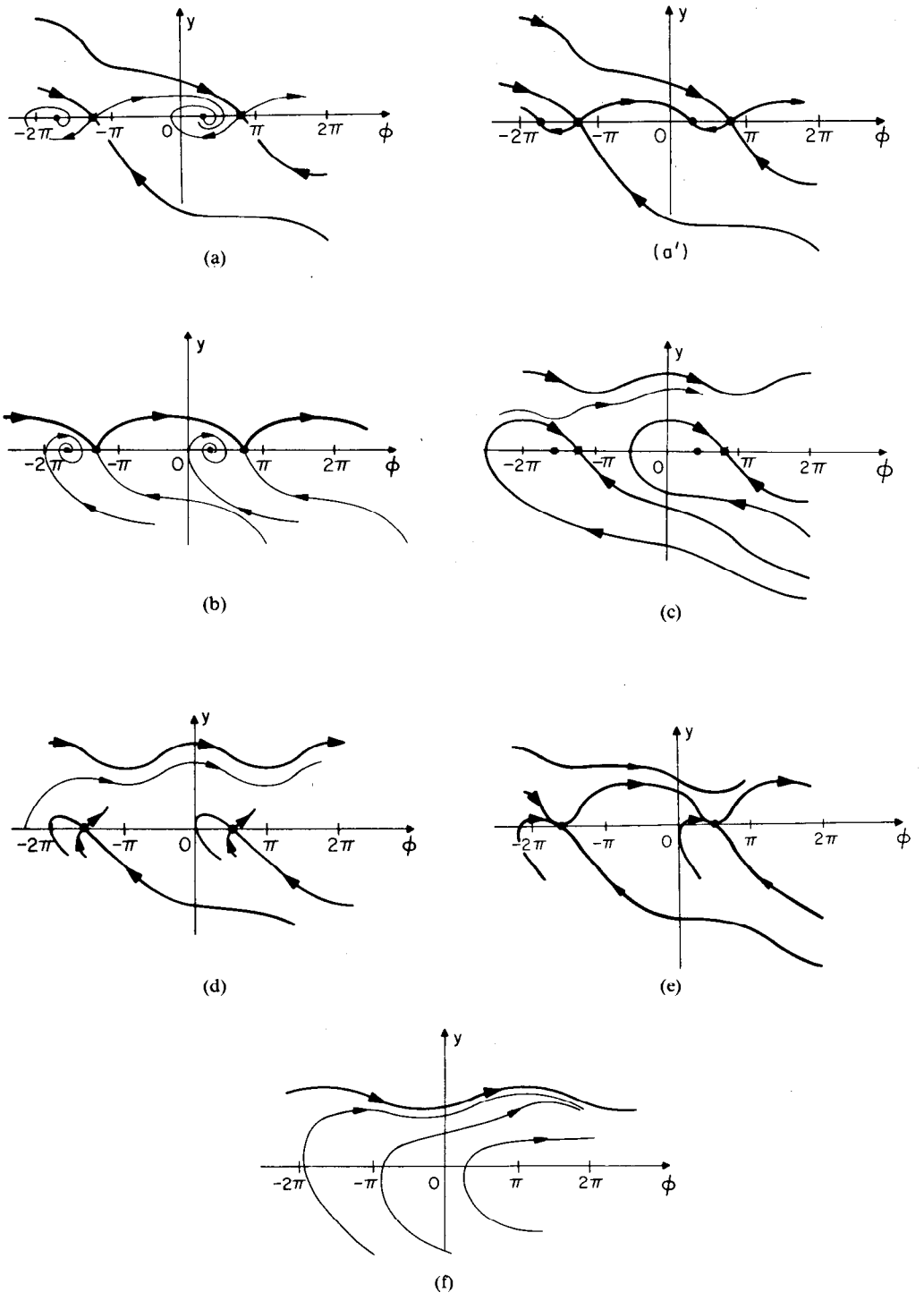

Fig. 3. (a) The completely stable case. (a') Homeomorphic to Fig. 3(a) —the stable equilibria are nodes rather than foci. (b) The saddle connection bifurcation. (c) One stable rotation and two equilibrium points. (d) Saddle-node bifurcation. (e) Simultaneous saddle-node and saddle connection bifurcation. (f) Single rotation and no equilibrium points.

2.3. *Sinusoidal Forcing (AC Analysis)*

This is the case of primary interest to us in this paper, namely, (2.3) with $i_s(\tau) = \rho + \epsilon A' \sin \bar{\omega}\tau$ (bias + small sinusoidal forcing). It is the model for the dynamics of the Josephson junction when used in microwave generators and mixers [7,13,16]. In standard first-order form, (2.3) now reads

$$\dot{\phi} = y, \quad \dot{y} = \frac{-y - \sin\phi + \rho + \epsilon A' \sin \bar{\omega}\tau}{\beta}. \tag{2.7}$$

A variation of (2.7) was first studied by Belykh, Pedersen, and Soerensen [7]. Their work was thorough but primarily qualitative (i.e., analytic details are often absent). Abidi

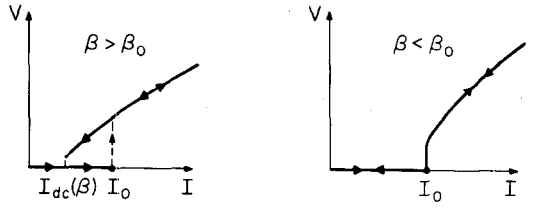

Fig. 4. $I-V$ characteristics of the Josephson junction: (a) Hysteresis curve corresponding to line (A) in the bifurcation diagram of Fig. 2. (b) No hysteresis curve corresponding to line (B) of Fig. 2.

and Chua [3] studied analytically the case when $\beta = 0$ (zero junction capacitance) and ϵ not necessarily small—in this case (2.7) simplifies to

$$\dot{\phi} = \rho - \sin\phi + \epsilon A' \sin \bar{\omega}\tau \tag{2.8}$$

a first-order equation periodic in both ϕ and τ and hence considered as a flow on a torus. The rotation number technique was then applied (see Pliss [15]). Odyniec and Chua [13] showed in analytical detail that the conclusions of [3] are valid not only for $\beta = 0$ but also for small β by using perturbation arguments to show that the (stable) invariant torus associated with (2.8) is perturbed to a stable invariant torus (for a sufficiently small β) which attracts trajectories of (2.7). They also treated the case when ϵ is small and β is large so as to satisfy $\beta > \beta_0$ and $\rho > \rho_c(\beta)$. Such a β lies in regions (c) or (f) in the diagram of Fig. 2, and hence the phase portrait of the dc forced Josephson junction possesses a stable rotation.

The work of Belykh *et al.* [7] treats a slightly more general form of (2.7), namely,

$$\dot{\phi} = y,$$
$$\dot{y} = \frac{1}{\beta}\left[\rho - (1 + \gamma\cos\phi)\, y - \sin\phi + \epsilon_1 \sin\bar{\omega}\tau\right]. \tag{2.9}$$

2.3.1. The AC Bifurcation Diagram of Belykh et al. [7]: Figs. 5, 6 are reproduced from [7], with the parameter γ in (2.9) assumed nonzero. Fig. 5 is a bifurcation diagram in the parameters β, ρ (with γ fixed)—a section of the 3-dimensional bifurcation diagram in β, ρ, γ. Fig. 6 displays topologically different portraits (of the Poincaré map) numbered corresponding to different regions of Fig. 5. (Since Fig. 5 is symmetric across the β axis, it is drawn only for $\rho \geq 0$).

To discuss Figs. 5 and 6 consider rewriting (2.9) as

$$\dot{\phi} = y$$
$$\dot{y} = \frac{1}{\beta}\left(-(1 + \gamma\cos\phi)\, y - \sin\phi + \rho + \epsilon_1 \sin\theta\right)$$
$$\dot{\theta} = \bar{\omega}. \tag{2.10}$$

θ is assumed to lie not on R but on an interval $[0, 2\pi]$ with 0 and 2π identified, i.e., $\theta \in S^1$. Now (2.10) is an autonomous system which is periodic in ϕ, and θ (with period

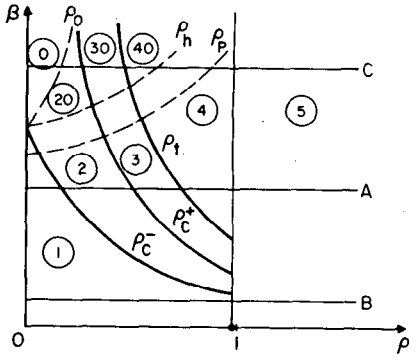

Fig. 5. Ac bifurcation diagram of (7).

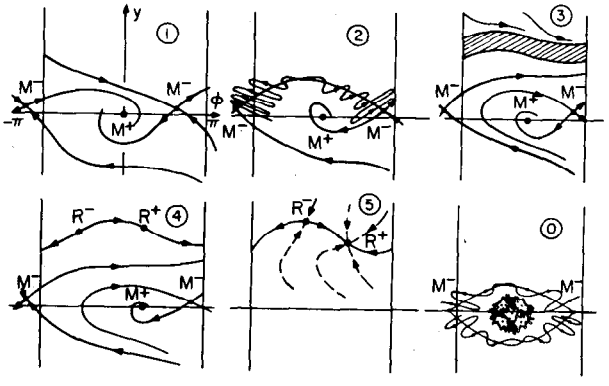

Fig. 6. Protraits of the Poincaré map for different regions of Fig. 5.

2π). Consider now the map

$$P(\tau_0)\colon (\phi(\tau_0), y(\tau_0), \theta(\tau_0)) \to \left(\phi\left(\tau_0 + \frac{2\pi}{\bar{\omega}}\right), y\left(\tau_0 + \frac{2\pi}{\bar{\omega}}\right), \theta\left(\tau_0 + \frac{2\pi}{\bar{\omega}}\right)\right):$$

i.e., in the change in ϕ, y, θ during one period of the forcing. Since the system (2.10) is autonomous the map $P(\tau_0)$ is the same for all τ_0. Further since $\theta(\tau_0 + (2\pi/\bar{\omega})) = \theta(\tau_0) \bmod 2\pi$, we need only concentrate on the map

$$P\colon (\phi(\tau_0), y(\tau_0)) \to \left(\phi\left(\tau_0 + \frac{2\pi}{\bar{\omega}}\right), y\left(\tau_0 + \frac{2\pi}{\bar{\omega}}\right)\right)$$

for some τ_0. This map is referred to as the period-one or *Poincaré map*. As before we can define the Poincaré map P either from $R^1 \times R^1$ to itself, or $S^1 \times R^1$ to itself. The Poincaré map contains all the information about the dynamics of (2.9), e.g., a fixed point of the Poincaré map P: $R^1 \times R^1$ to itself corresponds to an oscillation of the system (2.9) and a fixed point of the Poincaré map P: $S^1 \times R^1$ to itself which is not a fixed point of P: $R^1 \times R^1$ to itself corresponds to a rotation of the system (2.9). For further discussion of Poincaré maps see, for instance, [1], [9], [10].

We now discuss the bifurcation diagram of Fig. 5 in terms of the map P. Consider first traversing the bifurcation diagram 5 along line A. The portrait of the Poincaré map P, thought of now as a discrete dynamical system ([9]), in region ① is shown in Fig. 6①. On $S^1 \times R^1$, the map P has two fixed points, a stable fixed point M^+ and

an unstable (saddle) fixed point M^-. These are the only critical elements of P and all initial conditions converge to one or the other of these points. Thus the system (2.9) has only a *stable oscillation* (corresponding to M^+) and an *unstable oscillation* (corresponding to M^-). The stable and unstable manifolds of M^- are shown in Fig. 6①. In region ②, the map still has only two critical points M^+ and M^- on $S^1 \times R^1$. However, the "upper" stable and "upper" unstable manifolds of M^- and its replica intersect each other transversally once (and hence infinitely often). This intersection implies the existence of infinitely many (unstable) periodic as well as uncountable nonperiodic orbits for the equation (2.9), referred to as the *horseshoe* kind of *chaos*. (The description, physical meaning and interpretation of this kind of chaos is discussed in Section III, see also [1], [9], [10], [12]). On the boundary from regions ① to ② and regions ② to ③, the intersection between the stable and unstable manifolds of M^- is tangential rather than transversal (this case is not completely understood, see, however, Guckenheimer and Holmes [9]). Region ③ is associated with the Poincare section of Fig. 6③. It shows a shaded ring shaped region. The ring is an attracting set which contains *infinitely many stable* solutions. According to [7] little is known about the ring and its dynamics. We will show in Section VI that this ring is absent, for the parameter range shown, when γ in (2.9) is equal to zero. In region ④, there are stable and unstable fixed points corresponding to periodic orbits both of the *oscillation* and *rotation* type. Fig. 6④ shows two fixed points of the rotation type (R^- and R^+) and two of the oscillation type (M^- and M^+). In region ⑤ there are only periodic orbits of the rotation type. We elaborate on the dynamics in this region:

Fig. 6⑤ shows the presence of a stable (attracting) invariant curve containing R^- and R^+. This corresponds to the existence of a two dimensional stable (attracting) invariant surface for (2.9). This surface is periodic in ϕ and θ and so is diffeomorphic to a two-torus. The study of orbital behavior on a two dimensional torus is treated through the use of *rotation number* μ (see Pliss [15]), i.e., the ratio of the number of rotations in ϕ to the number of rotations in θ. In [3], [13] it is shown that $\langle y \rangle$ is proportional to μ. It can be shown [7], [13] that the structurally stable rotation numbers are rational, i.e., $\mu = p/q$; with $p, q \in Z_+$—this, of course, corresponds to a periodic solution on the torus.

The lowest horizontal line B in Fig. 5 crosses only the two distinct regions ①, ⑤. For large values of β (corresponding to small values in the damping $d = \beta^{-1/2}$ if model (2.4) is used) new regions emerge. Along line C, for small values of ρ we enter the region ⓪. Fig. 6⓪ shows a Poincaré section for this region. It can be envisioned as having both the "upper" and "lower" stable and unstable manifolds of the right hand replica of M^- intersecting, transversally, the "upper" and "lower" unstable and stable manifolds of the left hand replica of M^-, respectively. Note the resemblance to Fig. 6②, as well as the additional feature of transversal intersection of the "lower" stable and unstable manifolds. Further, within this loop of intersecting manifolds surrounding M^+ there is an alternating sequence of saddles and stable fixed points of the Poincaré map with the manifolds associated with the saddles intersecting each other transversally. This extremely complicated form of horseshoe chaos is explained in Section IV and Fig. 11 (see [9]). For the purpose of our presentation, we term this chaos as *doubly chaotic*. This would imply now, for larger values of ρ, the presence of more critical elements than in Fig. 6②, ④ corresponding to regions ②, ④. Proceeding along the line C we encounter the regions ⑳, ㉚, and ㊵ which have the same configurations as the portraits of Figs. 6②, ③, and ④, respectively, with the added presence of an alternating sequence of stable and saddle fixed points surrounding the stable fixed point as in Fig. 6⓪. The curves ρ_0, ρ_c^+, ρ_t, ρ_h separate the regions ⓪, ⑳, ㉚, ㊵, and ④ respectively.

2.3.2. The $I-V$ Characteristic:

Fig. 7(a), reproduced from [7], shows an $I-V$ characteristic corresponding to a junction having an intermediate value for β (the line A in Fig. 5). The experiment that gives rise to Fig. 7(a) consists of gradually increasing I_{dc} and measuring V_{av} for a junction having an intermediate value of β, i.e., traversing line A of Fig. 5 from left to right and then decreasing I_{dc}. Consider first the case of increasing I_{dc}:

In the region ①, almost all initial conditions will converge to the stable oscillation M^+ with time averaged $y = 0$. In the region ② ($\rho > \rho_c^-$), we have in addition to the oscillations M^+ and M^-, an infinite number of unstable rotations corresponding to the transversal intersection of the stable and unstable manifolds of M^-. However, since the initial conditions are close to the stable oscillation of M^+, with zero average value, we still get $V_{av} = 0$. The same argument explains, $V_{av} = 0$ in the region ③. In region ④, we have the stable oscillation M^+ as well as, for instance as in Fig. 6④, a stable rotation, R^+, however, the initial condition causes the junction to stay locked at M^+ with $V_{av} = 0$. In region ⑤, the oscillations disappear and the circuit locks onto a rotation in Fig. 6⑤ it would be the stable rotation R^+, with nonzero average value of y (proportional to the (stable) rotation number $\mu = p/q$). Now as I_{dc} increases, the voltage stays constant (since the rotation is stable) for small variations in I_{dc} (or ρ) and changes (jumps) in rational steps corresponding to changes in the rotation number. This part of the $I-V$ characteristic is the central theme of [3], [13], [14] shown in Fig. 7(b) as discontinuous and stepwise constant graph. Further, the heights of the steps are rationally related.

We now consider the case of decreasing I_{dc} where the hysteresis appears. As $\rho(I_{dc})$ is decreased, we drop from region ⑤ to region ④, initial conditions will keep the junction locked to a rotation and yield piecewise constant $I-V$ characteristic as in region ⑤. Decreasing ρ into

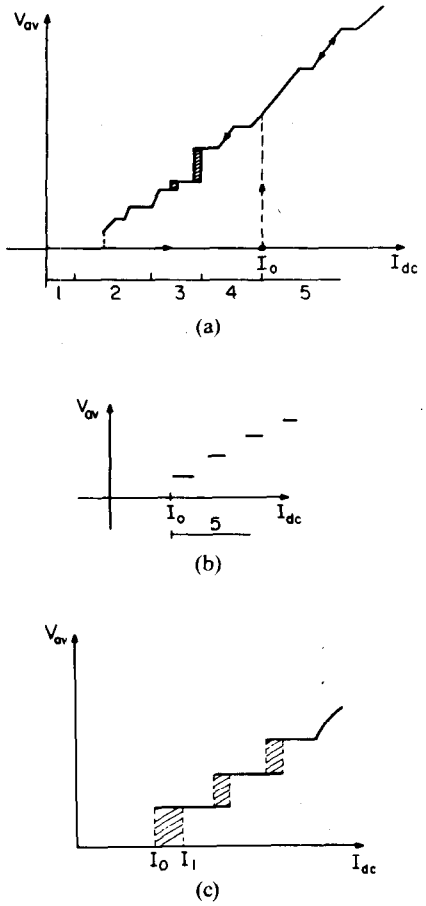

Fig. 7. (a) $I-V$ characteristic of an ac forced Josephson junction from (7). On the I_{dc} axis the extent of the regions 1, 2, 3, 4, 5 of Fig. 5 are shown. (b) Showing stepwise discontinuous and piecewise-constant characteristic in region 5. (c) Shaded regions in the $V_{av}-I_{dc}$ curve of (6). Chaos was observed via simulations for $\rho = 0.7155$, $\beta = 8.5$.

region ③, the circuit locks into the ring of solutions shown in Fig. 6③ yielding the unsettled $V_{av}-I_{dc}$ characteristic shown hatched in Fig. 7(a). In region ②, the chaotic region, the circuit locks into the infinitely many unstable rotations (or uncountable nonperiodic steady states) associated with the transversal intersection of Fig. 6②. Each of these have almost identical nonzero, average voltages. All these steady states are unstable and lie close to the domain of attraction of M^+. The circuit, therefore, could jump to the domain of attraction of the stable oscillation M^+, resulting in zero V_{av}, before traversing the boundary from region ② to region ①. At any rate, there is a sharp increase in the amount of perceived noise in the junction while in region ②. This is particularly deleterious in application of the junction as a mixer. Some authors show the instability of V_{av} values in the chaotic region ②, shaded on the $V_{av}-I_{dc}$ curve, as shown in Fig. 7(c), taken from [6].

2.4. *Our Contribution*

We have discussed in Section 2.3 the qualitative and simulation work of [7] and the limited analytic work of [3], [13], [14]. In the rest of this paper we prove rigorously those conclusions of [7] that have not been proven in [3], [13], [14]. The model we consider is (2.7) with $\gamma = 0$. Since the discussion of regions ④ and ⑤ is more or less complete, we focus in the next four sections on regions ⓪, ② and ③. We establish the existence of Region ⓪ in Section IV and Region ② in Section V. We collect the conclusions of these two sections in Section VI where we also establish that region ③ is absent when $\gamma = 0$ (for the shown parameter ranges in Fig. 5), and the connection between the ac and dc bifurcation diagrams.

We would like to emphasize that with these proofs an essentially comprehensive analytic picture of the dynamics emerges. We start with a brief review of our major technique: the Melnikov Method.

III. Chaos and the Melnikov Method

Chaos is a form of complicated behavior in the dynamics of deterministic nonlinear systems. Some varieties of complex behavior are now fairly known—aperiodic solutions, Birkhoff–Smale horseshoes, strange attractors, Arnold diffusion, overlapping of resonances, etc. Chaos entails orbital motion which is reminiscent of noise in that it possesses a broadband spectrum. A dynamical system undergoing chaos may simultaneously possess countably infinite number of periodic orbits and uncountably many recurrent motions which are not periodic. These motions emanate from certain regions in the phase space; moreover, they are extremely sensitive to variations in initial conditions. This extreme sensitivity is exhibited in the form of an uncertainty—over time, two initial conditions starting very close may diverge from one another exponentially (see [1], [9] for further discussion).

The majority of cases in which chaos has been reported in the literature are based on simulation or intuitive arguments. One specific form of chaos, the Smale horseshoe and its generalization, the Arnold diffusion has shown itself to be well suited to analysis and has been studied in, for instance, [1], [8]–[10]. We relegate the details of the horseshoe to these references.

The important conclusion of the presence of a horseshoe in the dynamics of a system is that it implies the onset of chaotic motion often referred to as "horseshoe chaos". Further a technique called the Melnikov technique provides an analytical tool for measuring the presence of the horseshoe chaos in certain periodically forced nonlinear systems. In ingenuous form, it gives information about the behavior of the perturbed periodic system based on a calculation involving trajectories of the unperturbed system. We review the method following [1], [8], [9].

Consider the system

$$\dot{x} = f(x) + \epsilon g(x, t) \tag{3.1}$$

where f, g are sufficiently smooth functions; f from R^2 to R^2; and g from R^3 to R^2 is T-periodic in t. The associated unperturbed system is

$$\dot{\bar{x}} = f(\bar{x}). \tag{3.2}$$

Assume that the system (3.2) possesses a homoclinic orbit. $\bar{x}_0(t)$, i.e., an orbit that connects a saddle equilibrium point x_0 to itself. From [8] it can be shown that for ϵ small

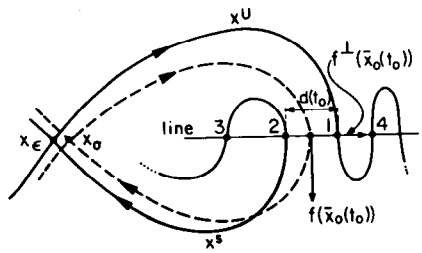

Fig. 8. Showing the perturbation of the homoclinic orbit and the definition of $d_\epsilon(t_0)$.

enough, the saddle equilibrium point x_0 gets perturbed to a saddle fixed point x_ϵ of the time-T Poincaré map of (3.1) as shown in Fig. 8. Let the perturbed stable orbit of x_ϵ be denoted $x^s_\epsilon(t, t_0)$ and the perturbed unstable orbit $x^u_\epsilon(t, t_0)$. Then the following lemmas are proven in [8], [9].

Lemma 3.1

$$x^u_\epsilon(t, t_0) = \bar{x}_0(t - t_0) + \epsilon x^{1u}(t, t_0) + 0(\epsilon^2),$$
$$\text{uniformly in } t \text{ for } t \in]-\infty, t_0]$$
$$x^s_\epsilon(t, t_0) = \bar{x}_0(t - t_0) + \epsilon x^{1s}(t, t_0) + 0(\epsilon^2),$$
$$\text{uniformly in } t \text{ for } t \in [t_0, \infty[.$$

Lemma 3.2 (First Variation Equations)

$$\dot{x}^{1u}(t, t_0) = D_{\bar{x}} f(\bar{x}_0(t - t_0)) x^{1u}(t, t_0) + g(\bar{x}_0(t, t_0), t) \quad \text{for } t \in]-\infty, t_0] \tag{3.3}$$

$$\dot{x}^{1s}(t, t_0) = D_{\bar{x}} f(\bar{x}_0(t - t_0)) x^{1s}(t, t_0) + g(\bar{x}_0(t - t_0), t) \quad \text{for } t \in [t_0, \infty[. \tag{3.4}$$

The separation between $x^u_\epsilon(t, t_0)$ and $x^s_\epsilon(t, t_0)$ (see Fig. 8) is measured by

$$d_\epsilon(t_0) = \frac{f(\bar{x}_0(0)) \wedge [x^u_\epsilon(t_0, t_0) - x^s_\epsilon(t_0, t_0)]}{|f(\bar{x}_0(0))|} \tag{3.5}$$

where $\wedge$ stands for the wedge product. The first variation of the distance $d_\epsilon(t_0)$ can be written as

$$d_\epsilon(t_0) = \frac{\epsilon M(t_0)}{|f(\bar{x}_0(0))|} + 0(\epsilon^2) \tag{3.6}$$

where $M(t_0)$ is the Melnikov function given by

$$M(t_0) = f(\bar{x}_0(0)) \wedge [x^{1u}(t_0, t_0) - x^{1s}(t_0, t_0)]. \tag{3.7}$$

The interest in evaluating the distance between $x^u_\epsilon(t, t_0)$ and $x^s_\epsilon(t, t_0)$ arises from the fact that if they intersect transversely once, they intersect each other infinitely often, as shown in Fig. 9, forming the so-called Smale horseshoe in the dynamics of the Poincaré map with countably many unstable orbits of different periods as well as aperiodic recurrent orbits. The Melnikov method evaluates $M(t_0)$, the first variation in the distance $d_\epsilon(t_0)$ scaled by $|f(\bar{x}_0(0))|$. Consequently, if the function $M(t_0)$ has transversal zeros, i.e., if $\exists \tilde{t}_0$ such that

$$M(\tilde{t}_0) = 0, \qquad \frac{dM}{dt_0}(\tilde{t}_0) \neq 0$$

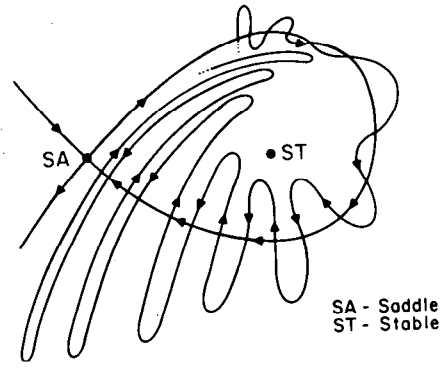

Fig. 9. The Poincaré map of a perturbed homoclinic orbit showing infinitely many intersections of the stable and unstable manifolds.

it follows that $x^u_\epsilon(t, t_0)$ and $x^s_\epsilon(t, t_0)$ intersect transversally once (and hence infinitely often) resulting in the horseshoe chaos. To obtain an expression for $M(t_0)$ we write (3.7) as

$$M(t_0) = \Delta^u(t_0, t_0) - \Delta^s(t_0, t_0) \tag{3.8}$$

where

$$\Delta^u(t, t_0) := f(\bar{x}_0(t - t_0)) \wedge x^{1u}(t, t_0), \quad \text{for } t \in]-\infty, t_0] \tag{3.9}$$

and

$$\Delta^s(t, t_0) := f(\bar{x}_0(t - t_0)) \wedge x^{1s}(t, t_0), \quad \text{for } t \in [t_0, \infty[. \tag{3.10}$$

Using (3.3) and (3.4), obtaining (3.8) becomes a final (resp. initial) value problem for the differential equation satisfied by $\Delta^u(t, t_0)$ (res. $\Delta^s(t, t_0)$); namely,

$$\frac{d}{dt}\Delta^u(t, t_0) = \dot{f} \wedge x^{1u} + f \wedge \dot{x}^{1u}$$
$$= [\text{trace} D_{\bar{x}} f(\bar{x}_0(t - t_0))] \Delta^u + f(\bar{x}_0(t - t_0)) \wedge g(\bar{x}_0(t - t_0), t), \quad \text{for } t \in]-\infty, t_0] \tag{3.11}$$

$$\frac{d}{dt}\Delta^s(t, t_0) = [\text{trace } D_{\bar{x}} f(\bar{x}_0(t - t_0))] \Delta^s + f(\bar{x}_0(t - t_0)) \wedge g(\bar{x}_0(t - t_0), t), \quad \text{for } t \in [t_0, \infty[. \tag{3.12}$$

Equations (3.11) and (3.12) are scalar linear time-varying differential equations which can be explicitly integrated to solve the final and initial value problems respectively. The values $\Delta^u(-\infty, t_0)$ and $\Delta^s(t_0, \infty)$ do not appear in the expression for $M(t_0)$ if $\Delta^u(t, t_0)$ approaches zero more rapidly than $\exp\{-\int_{t_0}^t \text{trace}[D_{\bar{x}} f(\bar{x}_0(s - t_0))]\, ds\}$ as $t \to -\infty$ and $\Delta^s(t, t_0)$ approaches 0 more rapidly than $\exp\{-\int_{t_0}^t \text{trace } D_{\bar{x}} f(\bar{x}_0(s - t_0))\, ds\}$ as $t \to \infty$. Under this condition, (the "exponential convergence" condition, see [1]), we may write, by integrating (3.11) and (3.12) and substituting in (3.8),

$$M(t_0) = \int_{-\infty}^{\infty} f(\bar{x}_0(t)) \wedge g(\bar{x}_0(t), t + t_0) \cdot \exp\left[-\int_0^t \text{trace } D_{\bar{x}} f[\bar{x}_0(s)]\, ds\right] dt. \tag{3.13}$$

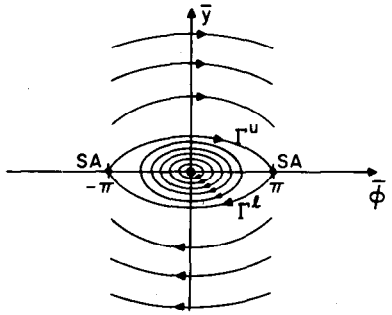

Fig. 10. Phase portraits of the unperturbed unforced Hamiltonian system.

This is the Melnikov Integral. When the unperturbed system is Hamiltonian, trace $D_{\bar{x}} f(\bar{x}_0(s)) \equiv 0$ so that the Melnikov integral of (3.13) is valid without any further conditions.

Generally speaking the Melnikov technique has been used to establish chaos in periodic perturbations of Hamiltonian systems. In Section V, we will apply the Melnikov technique in a novel way to the non-Hamiltonian Josephson junction circuit model of Section II.

IV. Chaos in the Josephson Junction Dynamics: The Close to Hamiltonian Case

In this section we study the Josephson junction equation where the conductance G and the dc forcing I_{dc} are small. The transformation taking (2.1) to (2.3) is singular in the limit that $G = 0$. Hence, we will use the scaling of (2.4), viz.

$$\ddot{\phi} + d\dot{\phi} + \sin\phi = i_s'(t'). \tag{4.1}$$

$i_s'(t')$ is of the form $\epsilon(\rho' + A'\sin\omega' t')$ and $d = \epsilon d_0$, where $\omega' = (\bar{\omega}/d)$ and ϵ is a small parameter. We will show that in this form (4.1) possesses a Smale horseshoe in its dynamics. The parameter ranges studied in this section correspond to the large β, small ρ part of the bifurcation diagram of Fig. 5.

The unperturbed system (for $\epsilon = 0$) is

$$\begin{aligned} \dot{\bar{\phi}} &= \bar{y} \\ \dot{\bar{y}} &= -\sin\bar{\phi} \end{aligned} \tag{4.2}$$

(Notation consistent with Section III). Equations (4.2) are Hamiltonian with (energy) given by

$$H(\bar{y}, \bar{\phi}) = \left(\frac{\bar{y}}{2} - \cos\bar{\phi}\right). \tag{4.3}$$

There are two saddle connection orbits for this system, as shown in Fig. 10 labeled Γ^u (upper) and Γ^l (lower): strictly Γ^u and Γ^l are both homoclinic orbits, when we take into account the 2π-periodicity of (4.2) in $\bar{\phi}$.

The value of the Hamiltonian $H(\bar{y}, \bar{\phi})$ on these orbits is easily seen to be 1 and the orbits given explicity by

$$\begin{aligned} \bar{y}(t' - t_0) &= \pm 2\,\mathrm{sech}(t' - t_0) \\ \bar{\phi}(t' - t_0) &= \pm 2\arctan[\sinh(t' - t_0)] \end{aligned} \tag{4.4}$$

where the + sign is for Γ^u and the − sign is for Γ^l. The Melnikov integral (3.14) is specialized to this case to be

$$\begin{aligned} M(t_0) &= \int_{-\infty}^{\infty} \bar{y}(\rho' - d_0\bar{y} + A'\sin\omega'(t' + t_0))\,dt' \\ &= \int_{\mp\Pi}^{\pm\Pi} \rho'\,d\bar{\phi} - d_0\int_{-\infty}^{\infty} [\pm 2\,\mathrm{sech}\,t']^2\,dt' \\ &\quad + \left[\int_{-\infty}^{\infty} \pm 2\,\mathrm{sech}\,t' \cdot \cos\omega' t'\,dt'\right] A'\sin\omega t_0. \end{aligned} \tag{4.5}$$

(we have used here $(d\bar{\phi}/dt') = y$, and the fact that $\int_{-\infty}^{\infty} \mathrm{sech}\,t\,\sin\omega' t\,dt = 0$—integral of an odd function). Evaluating (4.5) explicitly yields

$$M(t_0) = \pm\rho' 2\pi - 8d_0 \pm A'\left[2\pi\,\mathrm{sech}\frac{\pi\omega'}{2}\right]\cdot\sin\omega' t_0 \tag{4.6}$$

For Γ^u, the upper homoclinic orbit, the separation

$$M^u(t_0) = 2\pi\rho' - 8d_0 + A'R(\omega')\sin\omega' t_0 \tag{4.7}$$

where $R(\omega') := 2\pi\,\mathrm{sech}(\pi\omega'/2) > 0$. For (4.7) to have a zero $\tilde{t}_0$, we see that it is necessary to have

$$|-2\pi\rho' + 8d_0| \leqslant A'R(\omega'). \tag{4.8}$$

It is easy to verify that the zero $\tilde{t}_0$ is *transverse* when the inequality is strict for any nonzero finite frequency ω'. When (4.8) becomes an equality, the zero $\tilde{t}_0$ is *nontransverse*.[4]

For $I_{dc}(:= I_0\rho)$ values satisfying (4.8), the upper homoclinic curve Γ^u breaks up as in Fig. 6② and hence implies the presence of a horseshoe chaos. Analogously for Γ^l the lower homoclinic orbit the Melnikov function

$$M^l(t_0) = -2\pi\rho' - 8d_0 - A'R(\omega')\sin\omega' t_0. \tag{4.9}$$

For (4.9) to have transversal zeros, it is necessary (and sufficient) to have

$$|2\pi\rho' + 8d_0| \leqslant A'R(\omega') \tag{4.10}$$

(and the strict inequality is satisfied).

When ρ' is such that both (4.8) and (4.10) are simultaneously satisfied for a fixed ω', we have the complicated phase portrait of Fig. 11 (note that if (4.10) is satisfied, then (4.8) is also satisfied). In addition to the "doubly chaotic" intersections of the stable and unstable manifolds of the saddle, there is within the loop of intersecting manifolds an alternating sequence of saddles and stable fixed points of the Poincaré map with the manifolds associated with the saddles intersecting each other transversally (overlapping of resonances)—a more comprehensive description of this portrait is in [9, pp. 222], for example.

The portrait of Fig. 11 persists for a continuum of 'small' ϵ values corresponding to small d (or to relate this to Fig. 5, large $\beta = d^{-2} = \epsilon^{-2}d_0^{-2}$). The conditions (4.8) and (4.10) enable us to derive the curves ρ_c^-, ρ_c^+ and ρ_0 of

[4] In this instance, one has to consider higher order terms in ϵ in the separation equation (3.6). In this case, some techniques due to Newhouse could be utilized, see [9].

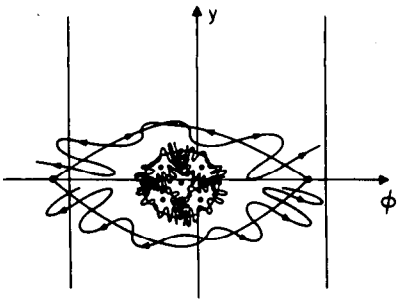

Fig. 11. Small periodic perturbation of the Hamiltonian system of Fig. 10—corresponding to the junction with high and intermediate values of β.

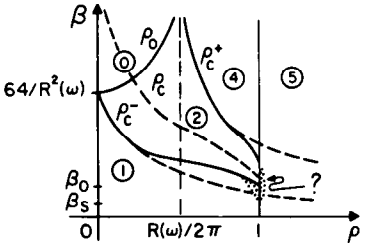

Fig. 12. The bifurcation diagram of system (2.9) when $\gamma = 0$.

Fig. 5 as follows:

First substitute $d_0 = (1/\epsilon)\beta^{-1/2}$, $\rho' = \rho/\epsilon$, and $A' = A/\epsilon$ into (4.8) and obtain

$$|-2\pi\rho + 8\beta^{-1/2}| \leq AR(\omega') =: \tilde{R}(\omega'). \tag{4.11}$$

Then we rewrite this equation as two separate conditions

$$\rho \geq \frac{1}{2\pi}\left[8\beta^{-1/2} - \tilde{R}(\omega')\right] =: \rho_c^- \tag{4.12a}$$

$$\rho \leq \frac{1}{2\pi}\left[8\beta^{-1/2} + \tilde{R}(\omega')\right] =: \rho_c^+. \tag{4.12b}$$

Note that for $\beta \to 0^+$ both ρ_c^- and $\rho_c^+ \to +\infty$. As β increases from 0 both ρ_c^- and ρ_c^+ decrease to finite values: at $\beta = (8/\tilde{R}(\omega'))^2$, $\rho_c^- = 0$ and as $\beta \to +\infty$, $\rho_c^+ \to \tilde{R}(\omega')/2\pi$. The curves ρ_c^- and ρ_c^+ are plotted in Fig. 12. Since the analysis of this section is valid only for large and intermediate values of β, the curves ρ_c^-, ρ_c^+ diverge from those predicted by (4.12a) and (4.12b) for smaller values of β. Hence in Fig. 12, we have shown the actual curves ρ_c^-, ρ_c^+ (the solid lines) diverge from the curves ρ_c^-, ρ_c^+ of (4.12a) and (4.12b) (the dotted lines) for small values of β. The discussion of the onset of chaos in the small β case is in Section V.

We now derive the expression for the curve ρ_0 corresponding to region ⓪; here (4.10) holds, and hence (4.8) does also, and it gives the equation for ρ_0 as follows: rewrite (4.10) as

$$|2\pi\rho + 8\beta^{-1/2}| \leq AR(\omega') =: \tilde{R}(\omega'). \tag{4.13}$$

For ρ and β postive, (4.13) yields one useful condition,

$$\rho \leq \frac{1}{2\pi}\left[\tilde{R}(\omega') - 8\beta^{-1/2}\right] =: \rho_0. \tag{4.14}$$

At $\beta = (8/\tilde{R}(\omega'))^2$, ρ_0 coincides with the curve ρ_c^-, i.e., $\rho_0 = 0$. As β increases so does ρ_0; and as $\beta \to +\infty$, $\rho_0 \to \tilde{R}(\omega')/2\pi$ as does the curve ρ_c^+. The curve ρ_0 is plotted in Fig. 12 also. Note that $\tilde{R}(\omega') := 2\pi A \operatorname{sech}(\pi\omega'/2)$. That is, for a fixed (small) A the choice of the frequency ω' determines the quantity $R(\omega')$ which in turn determines the width of region ② in Fig. 12. (The frequency ω' is the normalized frequency of the periodic ac-forcing.)

The other curves ρ_h, ρ_p of Fig. 5 can also be obtained at least qualitatively, if not explicitly, using the Melnikov technique to obtain conditions (i.e., inequalities) for the occurrence of the resonance of periodic orbits about the stable fixed point of the Poincaré map as shown in Fig. 6⓪ or Fig. 11. The usage of the Melnikov technique in the case of resonances is treated in [9], for instance.

We remark that the derived curves ρ_c^-, ρ_c^+, and ρ_0 are not the actual boundaries of the different regions in the bifurcation diagram even for small ρ, and large-β values; though at these ρ-β values, the curves are within order ϵ^2 of magnitude from the actual boundaries.

V. Chaos in the Josephson Junction Dynamics —the Non-Hamiltonian Case

We consider here the model of (2.7) and no small parameter assumptions except on the magnitude of the periodic forcing. The unperturbed system with $\epsilon = 0$ is given by

$$\dot{\bar{\phi}} = \bar{y}, \qquad \dot{\bar{y}} = \frac{-\bar{y} - \sin\bar{\phi} + \rho}{\beta}. \tag{5.1}$$

Let $\rho = \rho_c(\beta)$, i.e., the constant forcing is chosen such that the autonomous system has a homoclinic orbit, as in Fig. 3(b). The Melnikov integral (3.13) in this case is given by

$$M(t_0) = \int_{-\infty}^{\infty}\left[\bar{y}(t)\cdot\frac{A'}{\beta}\sin\bar{\omega}(t+t_0)\right]\cdot\exp\left(\frac{t}{\beta}\right)dt \tag{5.2}$$

(Note that the presence of the term $\exp(t/\beta)$ necessitates checking the exponential convergence condition of Section III—this is done in the Appendix). The integral (5.2) may be simplified to

$$M(t_0) = \frac{A'}{\beta}\left\{\left[\int_{-\infty}^{\infty}\bar{y}(t)e^{t/\beta}\sin\bar{\omega}t\,dt\right]\cos\bar{\omega}t_0 + \left[\int_{-\infty}^{\infty}\bar{y}(t)e^{t/\beta}\cos\bar{\omega}t\,dt\right]\sin\bar{\omega}t_0\right\}. \tag{5.3}$$

If the integrals in the square bracket exist, are finite and are not both zero, then one can easily show that transversal zeros exist (two in each period, $2\pi/\bar{\omega}$, in t_0) see, e.g., Kopell and Washburn [12], Salam *et al.* [27]). Our task is to show that these integrals do exist and are finite. Consider the integrals:

$$I_1(\bar{\omega}) := \int_{-\infty}^{\infty}\bar{y}(t)e^{t/\beta}\sin\bar{\omega}t\,dt$$

and

$$I_2(\bar{\omega}) := \int_{-\infty}^{\infty}\bar{y}(t)e^{t/\beta}\cos\bar{\omega}t\,dt. \tag{5.4}$$

Since $\bar{y}(t)$ is a bounded smooth function with $\bar{y}(t) \to 0$ as

$t \to \pm\infty$, it is enough to show that $\bar{y}(t)e^{t/\beta} \to 0$ fast enough as $t \to \pm\infty$ for the integrals (5.4) to be finite. Now $\bar{y}(t)$ is a component of $\bar{x}_0(t)$ the homoclinic orbit of the unperturbed system. Hence for t values close to $\pm\infty$, the rate of approach of $\bar{y}(t)$ to the saddle x_0 is given by the eigenvalues of the linearization of the vector field of the unperturbed system at the saddle equilibrium $x_0 = (\bar{\phi}_0, 0)$, i.e., the eigenvalues of

$$\begin{bmatrix} 0 & 1 \\ -\frac{1}{\beta}\cos\bar{\phi}_0 & -\frac{1}{\beta} \end{bmatrix} \tag{5.5}$$

where $\bar{\phi}_0$ satisfies $\rho = \sin\bar{\phi}_0$. The eigenvalues of (5.5) are, respectively,

$$\lambda^s = -\frac{1}{2\beta} - \frac{1}{2\beta}\left[1+4\beta(1-\rho^2)^{1/2}\right]^{1/2} < -\frac{1}{\beta} < 0$$

$$\lambda^u = -\frac{1}{2\beta} + \frac{1}{2\beta}\left[1+4\beta(1-\rho^2)^{1/2}\right]^{1/2} > 0 \tag{5.6}$$

where λ^s is the negative (stable) eigenvalue and λ^u the positive (unstable) eigenvalue of the saddle equilibrium point x_0. As $t \to \infty$, $\bar{y}(t)$ approaches 0 as $e^{\lambda^s t}$; while as $t \to -\infty$, $\bar{y}(t)$ approaches 0 as $e^{\lambda^u t}$. Thus the quantity $\bar{y}(t)e^{t/\beta}$ is of the order of $\exp(\lambda^s + (1/\beta))t$ as $t \to \infty$ and of the order of $\exp(\lambda^u + (1/\beta))t$ as $t \to -\infty$. From (5.6) it follows that $\bar{y}(t)e^{t/\beta}$ goes to zero exponentially as $t \to \pm\infty$. Hence the integrals in (5.4) are well defined and finite. The Melnikov integral of (5.3) is thus well defined. The only thing that needs to be shown is that $I_1(\bar{\omega})$ and $I_2(\bar{\omega})$ are not both zero at all but discretely many frequencies. This follows from the analyticity of the two integrals in $\bar{\omega}$. Precisely, $I_2(\bar{\omega}) - iI_1(\bar{\omega})$ is the Fourier transform (an analytic function of $\bar{\omega}$) of a function $\bar{y}(t)e^{t/\beta}$ which is not identically zero (for all t), see [12] and [1] and the references therein. We have thus shown that the Melnikov integral

$$M(t_0) = \frac{A'}{\beta}\left[I_1(\bar{\omega})\cos\bar{\omega}t_0 + I_2(\bar{\omega})\sin\bar{\omega}t_0\right]$$

has transversal zeros (two in every period) at all but a discrete set of $\bar{\omega}$'s. Two difficulties were overcome in using the Melnikov approach in this case (low β case): (1) The validity of the formula for $M(t_0)$ has to be verified by verifying the exponential convergence condition (Appendix), (2) The convergence of the improper integral (5.2) has to be verified and then examined for transversal zeros. Such questions must be addressed in any application of the Melnikov integrals. (Only question (2) arises in the Hamiltonian case).

We have shown the presence of the horseshoe chaos for $\rho = \rho_c(\beta)$. Since the horseshoe is structurally stable,[5] chaos persists for small variations in ρ and β about $\{(\beta, \rho): \rho = \rho_c(\beta), \beta \geq \beta_0\}$. The curve ρ_c is shown dotted in Figure 12 relative to ρ_c^-, ρ_c^+; and as expected it lies between ρ_c^- and ρ_c^+. For large values of β the analysis of Section IV established chaos. For smaller values of β close to β_0; one can only say that a neighborhood of the curve ρ_c exhibits the horseshoe chaos and the boundaries of chaotic region (2) differ appreciably from the ρ_c^- and ρ_c^+ of (4.12a) and (4.12b). We expect that the *neighborhood of the curve* ρ_c where chaos is encountered *shrinks as* $\beta \to \beta_0$. That is so since smaller values of β (large values of damping d) increase the rate of convergence of trajectories starting off the saddle connection (of the unperturbed system) away from the saddle connection, see Fig. 3(b).

[5] Precisely, structural stability implies the property, i.e., chaos persists for an (open) neighborhood of vector fields which in turn contains the (ρ, β)-parameterized vector fields.

VI. Conclusions: Transition from the DC to the AC Bifurcation Diagram

In this section we combine the results of Sections IV and V with those of [3], [13], [14] to establish the transition from the dc to the ac bifurcation diagram.

We study the transition from the dc bifurcation along line (A) of Fig. 2, to line (A) of Fig. 5. For low values of ρ, we are in region (a) of Fig. 2 corresponding to one stable equilibrium point and one saddle (both hyperbolic). Under small periodic perturbation (ϵ small) it is elementary (see [9]) to show that the stable equilibrium point changes to a *stable oscillation* and the saddle equilibrium to a *saddle oscillation* (both hyperbolic). The average value of y on both these orbits is zero. (Corresponding to zero average voltage in the steady state).

For $\rho > \rho_c(\beta)$ a stable (hyperbolic) rotation appears in the dc dynamics both in the interior of regions (c) and (f) as shown in Fig. 3(c) and (f). For the augmented dynamics of (2.5) with $(\phi, y, \theta) \in S^1 \times R^1 \times S^1$ this rotation appears as a stable (hyperbolic) two-dimensional invariant surface diffeomorphic to a two torus. Under sufficiently small periodic perturbation (ϵ small) to the augmented dynamics (equivalently (2.9) with $\gamma = 0$), this invariant surface is only deformed (diffeomorphically). The stable (attracting) orbits are those corresponding to a (stable) rational rotation number $\mu = p/q$, see [7], [13]. The average voltage is proportional to these rational number. When the rotation number μ is not rational any one of a set of average voltages may be observed in an experiment—in Fig. 7(a); from [7], a single diagonal line connecting the steps was observed: in Fig. 7(b) of [13], nothing is filled in between steps; while in Fig. 7(c) of [6] the space between steps is shown shaded. This situation corresponds to regions ④ and ⑤ of Fig. 12.

For $\rho = \rho_c(\beta)$ and small or intermediate values of β, the dc dynamics show a saddle connection, Fig. 3(b). We have shown how small periodic perturbations of this saddle connection result in the presence of the (horseshoe) chaos in Section V, and the appearance of region 2 in Fig. 12.

For β large and ρ small, the dc dynamics are near the Hamiltonian that has the phase portrait of Fig. 10. We showed how small periodic perturbation of this case results in the appearance of regions ⓪, ⑳, ㊵ in Section IV, we derived analytic expressions for ρ_c^-, ρ_c^+ and ρ_0 also. The geometric picture is that the periodic perturbation "splits" the curve $\rho_c(\beta)$ of Fig. 2 into the curves ρ_c^- and ρ_c^+, allowing the region of chaos to emerge as shown in Fig. 12.

Region (d) of the dc dynamics corresponding to $\rho = 1$ translates to a saddle-node bifurcation of the stable and saddle oscillations of the ac forced system.

Now, consider region (e) of the dc dynamics corresponding to Fig. 3(e) ($\rho = 1$, $\beta < \beta_0$). First for $\beta = 0$, the system (2.7) reduces to a two-dimensional system which exhibits no complicated behavior—and using singular perturbation theory [13] it is readily verified that this behavior persists for $\beta \leqslant \beta_s < \beta_0$. Thus the saddle-node of the dc dynamics translates to a saddle-node of "oscillations" in the ac dynamics; and the associated (nonhyperbolic) equilibria connection will not translate to (transversal) homoclinic behavior in the ac dynamics. The region $\beta_s \leqslant \beta \leqslant \beta_0$ is not susceptible to easy analysis by the Melnikov technique since the invariant manifold joining equilibria (cf. Fig. 3(e)) involves nonhyperbolic equilibrium points. We conjecture that since the curves ρ_c^-, ρ_c^+ start off as analytic functions of β (see (4.12) (a) and (b)), they should extend to part of the component of region (e) as shown dotted in Fig. 12.

Finally we state the following extensions in the form of two remarks. First; the qualitative, simulation and experiments based, study of Belykh, Pedersen, and Soerensen [7], as well as of [6] and [11], gives the range of the periodic perturbation parameter ϵ_1 which extends to (comparatively) large values—at these values the analytic tools available all become invalid. However, the physics literature contains numerous experimental and simulation studies which show that properties such as chaos persists and "strengthens" as ϵ extends beyond its analytic range (see [18]). This experimental work had focused on near-Hamiltonian Systems and chaos generated by nonanalytic ϵ is refered to as "Strong Stochasticity", where as for analytic ϵ the term "Weak Stochasticity" is used. It is reasonable to believe that chaos "strengthens" for larger ϵ; since the restriction on the analytic ϵ is set primarily to ensure the validity of the measuring technique, namely, the Melnikov method.

The second remark concerns the applicability of our results to power systems; namely, the 3-machine case as in Kopell and Washburn [12], and also in Salam, Marsen, and Varaiya [2]. In [12], the power system model is transformed to one that is identical to model (2.4), with damping d set to zero and $i_s'(t') = \rho + \epsilon_1 \sin(\omega' t')$—a perturbed Hamiltonian. The authors concluded the presence of chaos in this (perturbed) Hamiltonian system, then they offered qualitative arguments to ensure the chaotic dynamics persistence under the addition of small (positive) damping d. Our result of Section V supports, in an analytic rigor, their qualitative arguments; moreover it allows for the addition of a larger amount of damping.

Appendix I
Existence of the Melnikov Integral (5.2)

Recall that

$$\Delta^u(t, t_0) = f(\bar{x}_0(t - t_0)) \wedge x^{1u}(t, t_0).$$

x^{1u} satisfies a (bounded) linear time varying differential equation, i.e.,

$$\dot{x}^{1u}(t, t_0) = \begin{bmatrix} 0 & 1 \\ -\frac{1}{\beta}\cos\bar{\phi}_0(t) & -\frac{1}{\beta} \end{bmatrix} x^{1u}(t, t_0) + \begin{bmatrix} 0 \\ \frac{1}{\beta}\sin\omega t \end{bmatrix} \quad \text{(A.1)}$$

Now in order that the solution $x^{1u}(t, t_0)$ of (A.1), backward in time, be bounded for $t \in]-\infty, t_0]$, one needs to show that the vector $x^{1u}(-\infty, t_0)$ has finite entries. To that end recall that the saddle x_0 gets perturbed to the saddle x_ϵ. Then using the first equation in Lemma 3.1 and letting $t \to -\infty$, one obtains

$$x_\epsilon = x_\epsilon(-\infty, t_0) = x_0 + \epsilon x^{1u}(-\infty, t_0) + 0(\epsilon^2).$$

Here $\epsilon > 0$, x_ϵ and x_0 are finite elements; and hence so is $x^{1u}(-\infty, t_0)$. Thus it follows that $x^{1u}(t, t_0)$ is bounded for $t \in]-\infty, t_0]$.

On the other hand, $f(\bar{x}_0(t - t_0))$ tends exponentially to zero at the rate of $\exp(\lambda^u t)$ as $t \to -\infty$, where $\lambda^u > 0$ is the "unstable" eigenvalue of the saddle defined in (5.6). Furthermore trace $Df_{\bar{x}}(\bar{x}_0(t)) \equiv -1/\beta$ so that $\Delta^u(t, t_0)\exp(+t/\beta)$ tends exponentially to zero as $t \to -\infty$.

Similarly, note that

$$\Delta^s(t, t_0) = f(\bar{x}_0(t - t_0)) \wedge x^{1s}(t, t_0)$$

with $x^{1s}(t, t_0)$ bounded on $[t_0, \infty[$. Further, $f(\bar{x}_0(t - t_0))$ tends exponentially to zero at the rate of $\exp(\lambda^s t)$ as $t \to \infty$, where $\lambda^s < -1/\beta$, is the "stable" eigenvalue of the saddle, defined in (5.6). Hence, $\Delta^s(t, t_0)\exp(+t/\beta)$ tends exponentially to zero as $t \to \infty$.

This establishes the exponential convergence condition of Section III, and validates (5.2)

References

[1] F. M. A. Salam, J. E. Marsden, and P. P. Varaiya, "Chaos and Arnold diffusion in dynamical systems," *IEEE Trans. Circuits Syst.*, vol. CAS-30, pp. 697–708, Sept. 1983.

[2] F. M. A. Salam, J. E. Marsden, and P. P. Varaiya, "Arnold diffusion in the swing equations of a power system," *IEEE Trans. Circuits Syst.*, vol. CAS-31, pp. 673–688, Aug. 1984.

[3] A. A. Abidi and L. O. Chua, "On the dynamics of Josephson junction circuits," *Electronic Circuits Systems*, vol. 3, pp. 186–200, 1979.

[4] A. A. Andronov, S. E. Khaiken, and A. A. Vitt, *Theory of Oscillations*. New York: Pergamon, 1966.

[5] A. Arapostathis, S. Sastry, and P. Varaiya, "Global analysis of swing dynamics," *IEEE Trans. Circuits Syst.*, vol. CAS 29, pp. 673–679, 1982.

[6] E. Ben-Jacobi, I. Goldhirsch, Y. Imry, and S. Fishman, "Intermittent chaos in Josephson junctions," *Phys. Rev. Lett.*, vol. 49, pp. 1599–1602, 1982.

[7] V. N. Belynkh, N. F. Pedersen, and O. H. Soerensen, "Shunted Josephson-junction model I—The autonomous Case and II. The non-autonomous case," *Phys. Rev. B*, vol. 16, pp. 4853–4871, 1977.

[8] B. O. Greenspan and P. J. Holmes, "Homoclinic orbits subharmonics and global bifurcation in forced oscillations," in *Nonlinear Dynamics and Turbulence*, Ed. G. Barenhalt, Pitman, 1983.

[9] J. Guckenheimer and P. J. Holmes, *Nonlinear Oscillations, Dynamical Systems and Bifurcations of Vector Fields*, Appl. Math. Sci., 42, Springer-Verlag 1983.

[10] P. J. Holmes, "Averaging and chaotic motions in forced oscillations," *SIAM J. Appl. Math.*, vol. 38 pp. 68–80, and vol. 40, pp. 167–168, 1980.

[11] B. A. Huberman, J. P. Crutchfield, and N. H. Packard, "Noise phenomena in Josephson junctions," *Appl. Phys. Lett.*, vol. 37, pp. 750–752, 1980.
[12] N. Kopell and R. B. Washburn, "Chaotic motion in the two-degree-of-freedom swing equations," *IEEE Trans. Circuits Syst.*, vol. CAS-29, pp. 738–746, 1982.
[13] M. Odyniec and L. O. Chua, "Josephson-junction circuit analysis via integral manifolds," *IEEE Trans. Circuits Syst.*, vol. CAS-30, May 1983.
[14] M. Odyniec and L. O. Chua, "Josephson-junction circuit analysis via integral manifolds: Part II," Memo. UCB/ERL M83/12, Univ. of California, Berkeley, Mar. 1983.
[15] V. A. Pliss, *Nonlocal Problems of the Theory of Oscillations*. New York: Academic, 1966.
[16] T. Van Duzer and C. W. Turner, *Principles of Superconductive Devices and Circuits*. New York: Elsevier, 1981.
[17] M. Levi, C. Hoppensteadt, and W. L. Miranker, "Dynamics of the Josephson junction," *Quart. Appl. Math.*, pp. 167–198, July 1978.
[18] A. J. Lichtenberg and M. A. Lieberman, *Regular and Stochastic Motion*, *Appl. Math. Sci.* vol. 38, Springer-Verlag, Dec. 1982.
[19] F. M. A. Salam and S. S. Sastry, "The complete dynamics of the forced Josephson junction circuit: The regions of chaos", Memo. DUMEM SM 83/02, Dep. of Mechanical Eng. and Mechanics, Drexel Univ., Philadelphia, PA, Sept. 1983.
[20] F. M. A. Salam, and S. S. Sastry, "Summary of the complete dynamics of the Forced Josephson junction circuit: The regions of chaos," in *Proc. 1984 IEEE ISCAS*, Montreal Canada.
[21] Z. D. Genchev, Z. G. Ivanov, and B. N. Todorov, "Effect of a periodic perturbation on radio frequency model of Josephson junction," *IEEE Trans. Circuits Syst.*, vol. CAS-30, pp. 633–636, Sept. 1983.
[22] B. Greenspan and P. Holmes, "Repeated resonance and homoclinic bifurcation in a periodically forced family of oscillators," *SIAM J. Math. Anal.*, vol. 15, no. 1, Jan. 1984.

✠

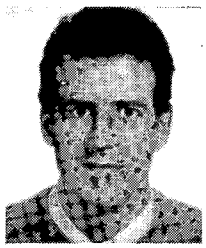

Fathi M. A. Salam received the M.S. degree in electrical engineering from the University of California, Davis, in 1979, the B.S. and Ph.D. degrees in 1976 and 1982, respectively, both in electrical engineering, and the M.S. degree in mathematics in 1982, from the University of California, Berkeley.

From 1976 to 1977 he worked for a subsidiary of Exxon in the instrumentation and maintenance division. He was a Visiting Assistant Professor of Electrical Engineering at the University of California at Berkeley, and is currently an Assistant Professor of Systems at Drexel University in the Department of Mechanical Engineering and Mechanics. His areas of current research interests are: nonlinear dynamical systems analysis, complicated dynamics, computer aided analysis; dynamics of Josephson junction circuits; and stability of interconnected power systems. He is currently an Associate Editor of IEEE TRANSACTIONS ON CIRCUITS AND SYSTEMS.

✠

S. Shankar Sastry (S'79–M'80) received the B. Tech degree from the Indian Institute of Technology, India, in 1977, and the M.S. and Ph.D. degrees in electrical engineering in 1979 and 1981, respectively, and the M.A. degree in mathematics in 1980, all from the University of California, Berkeley.

After having been on the faculty of the Massachusetts Institute of Technology, Cambridge, from 1980 to 1982, he is currently an Associate Professor in the Electronics Research Laboratory. University of California, Berkeley. His areas of research interest are nonlinear circuits and systems, applications of bifurcation and singular perturbation theory, adaptive control, kinematics, and dynamics of robots. He are an Associate Editor of the IEEE TRANSACTIONS ON CIRCUITS AND SYSTEMS and the *IMA Journal of Control and Information*. He received the President of India Gold Medal in 1977 and the IBM Faculty Development Award for 1983–1985.